Journal of Casting & Materials Engineering Vol. 6 No. 1 (2022) 1–7
https://doi.org/10.7494/jcme.2022.6.1.1

# The Correlation between Solidification Rates, Microstructure Integrity and Tensile Plastic Behaviour in 4.2 wt.% Silicon Strengthened Ductile Iron

**Giuliano Angella[a*], Marcello Taloni[a], Riccardo Donnini[a], Franco Zanardi[b]**

[a] Research Institute CNR-ICMATE, Department of Chemical Sciences and Materials Technology, via R. Cozzi 53, 20125 Milano (MI), Italy
[b] Zanardi Fonderie S.p.A., via Nazionale 3, 37046 Minerbe (VR), Italy
*e-mail: giuliano.angella@cnr.it*



Received: 26 October 2021/Accepted: 14 December 2021/Published online: 14 January 2022.
This article is published with open access at AGH University of Science and Technology Journals.

Paper presented at the EUROMAT 2021: Cast Irons and Steel Making. September 13–17, 2021, Virtual Conference.

**Abstract**

High Silicon Strengthened Ductile Iron (HSiSDI) with 4.2 wt.% of silicon was produced in Y-blocks with different thicknesses to investigate the effects of the solidification rate on microstructure integrity and tensile mechanical properties. With decreasing solidification rates, the graphite degeneracy with the appearance of chunky graphite became more significant at the highest silicon contents, so chemical ordering and graphite degeneracy seemed to be qualitative explanations of tensile property degradation. However, a deeper analysis of the relationship between solidification rate, microstructure and tensile properties was realized through an innovative approach based on the Matrix Assessment Diagram (MAD), where the parameters of Voce equation resulting from best-fitting the experimental tensile flow curves of a significant number of HSiSDI samples, were plotted. For 3.5 wt.% silicon content, the MAD analysis indicated that the microstructure was sound for any solidification rate, while for 4.5 wt.% the microstructure was sound only for the fastest solidification rates. For 4.2 wt.% silicon content the MAD analysis pointed out that the tensile plastic behaviour and the microstructure integrity was in between the 3.5 and 4.5 wt.% silicon contents, representing a composition threshold where the reliable microstructures were only found with the fastest solidification rates, while considerable variability was found for the slowest ones. Support to the MAD analysis results was given from microstructure observations.

**Keywords:**

strain hardening; constitutive equations; integrity assessment; ductile irons; high silicon content

## 1. INTRODUCTION

High Silicon Strengthened Ductile Irons (HSiSDIs) with alloying Si contents in the range 3.2–4.3 wt.% have recently been considered in the European Standard EN 1563:2018. They are fully ferritic because of the Si solid solution causing an increase of yield and tensile strengths with a moderate reduction of ductility [1–4], and a better machinability than ferritic and ferritic-pearlitic ductile irons with similar strengths [1, 2, 5–8]. However, besides the good balance of tensile properties, HSiSDIs impact resistance decreases significantly with increasing silicon alloying [9–12]. Indeed, tensile strength is maximum at 4.2–4.3 wt.% of Si content [4, 13, 14], and above this critical content both yield and tensile strength decrease rapidly, while ductility decreases rapidly above 3.5 wt.%, achieving zero ductility at about 5.0 wt.%, which has been attributed to progressive chemical ordering of the ferritic matrix with increasing silicon content. However, chunky graphite might also have a detrimental contribution to ductily as recently reported in [15]. Indeed, Si also promotes graphite degeneracy, resulting in a decrease in nodularity, and also the chunky graphite formation [4, 16–18]. Chunky graphite is commonly found in conventional ductile irons produced in heavy sections with slow solidification rates [18–22], where it has been reported a significant decrease of ductility and ultimate tensile strength [20, 21], although the most detrimental effect of chunky graphite is on the fatigue resistance [23, 24]. Futhermore other microstructure parameters like nodule count, size and roundness of the graphite nodules can affect the mechanical properties [3, 25–29].

Low structural integrity, i.e. metallurgical discontinuities and defects such as degenerated graphite, shrinkages, inclusions, etc., may have adverse effects on the final mechanical properties of ductile irons.

According to the literature [30–34] tensile tests are the simplest and useful experimental examinations for assessing the integrity of ductile irons. A new experimental method, namely the Voce approach, based on the mathematical modelling

of the tensile flow curves by means of the dislocation-density-related Voce constitutive equation, seems to allow the classification of the process-microstructure relations and the integrity assessment of different ductile irons grades [35–37]. The Voce equation is defined as:

$$\sigma = \sigma_V + (\sigma_0 - \sigma_V) \cdot \exp\left(\frac{\varepsilon_p}{\varepsilon_c}\right) \quad (1)$$

where:

- $\sigma$ – true flow stress;
- $\varepsilon_p$ – true plastic strain;
- $\sigma_V$ – saturation stress achieved asymptotically with plastic straining;
- $\sigma_0$ – back-extrapolated stress to $\varepsilon_p = 0$;
- $\varepsilon_c$ – characteristic transient strain that defines the rate with which $\sigma_V$ is achieved.

According to this approach, two diagrams are defined: the first one is the Matrix Assessment Diagram (MAD) graphically represented as $1/\varepsilon_c$ vs. $\Theta_o$, the Voce parameters obtained by fitting the differential experimental flow curves with the differential form of Equation (1), that is:

$$\frac{d\sigma}{d\varepsilon_p} = \Theta_o - \frac{d\sigma}{d\varepsilon_c} \quad (2)$$

MAD allows the univocal identification of different ductile iron grades, i.e. produced through different production routes and having different chemical composition, such as Austempered Ductile irons (ADI) and Isothermal Ductile Irons (IDI) [35–37]. The second diagram is called Integrity Assessment Diagram (IAD) and is represented by plotting the experimental elongation at failure vs. the theoretical one determined according to the Voce formalism. IAD appears to be able to identify the potential presence of defects.

The present paper is focused on the study of the effects of various cooling times on the tensile mechanical properties and microstructural integrity of different High Silicon Strengthened Ductile Iron (HSiSDI) samples with 4.2 wt.% of Si and manufactured through Y-blocks with different thicknesses. According to Voce approach, tensile flow curves were modelled using the constitutive Voce equation, and Voce parameters are derived from the best fittings. Knowing these parameters, MAD and IAD are represented and microstructural results are correlated.

## 2. EXPERIMENTAL

HSiSDI with nominal 4.2 wt.% of Si, which chemical composition is reported in Table 1, was produced by gravity pouring the molten metal through the pouring basin to the pattern plate in order to obtain three Y-block of 25, 50 and 75 mm thicknesses and a Lynchburg sample with diameter Ø = 25 mm complying with ASTM A 536-84(2019)e1. Thus, the different samples were produced under the same conditions. Therefore, it is worth mentioning that because of the different geometry and wall thickness of the molds, the cooling rate, which was not experimentally measured, changed between the four classes of samples.

**Table 1**
Chemical composition [wt.%]

| C | Si | Mg | Mn | P | S | Fe |
|---|---|---|---|---|---|---|
| 3.55 | 4.20 | 0.048 | 0.12 | 0.037 | 0.006 | Bal. |

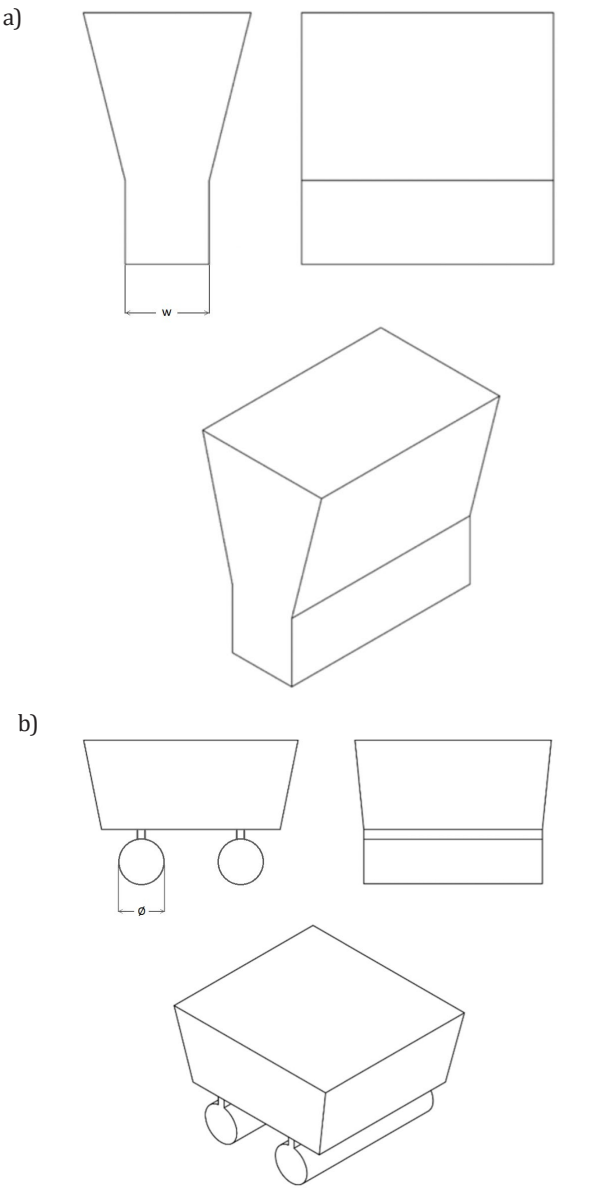


**Fig. 1.** Simplified representations of the molds used in the casting procedure: a) sketch of the three Y-molds, where the thickness w is equal to 25, 50, 75 mm respectively; b) sketch of the Lynchburg mold where the diameter Ø = 25 mm

A simplified representation of the Y-molds and Lynchburg mold is reported in Figure 1.

The microstructural characterization was performed using a Hitachi SU-70 high resolution scanning electron microscope. Through image analysis and complying with ASTM E2567-16a, nodule count, nodularity, mean diameter of graphite spheroids, area fractions of graphite and pearlite, and the presence of chunky graphite were found.

Tensile tests were carried out according to ASTM E8/E8M at strain rate $10^{-4}$ $s^{-1}$ on round specimens with initial gauge diameter $d_o$ = 12.5 mm and gauge length $l_o$ = 50 mm.

## 3. RESULTS

### 3.1. Microstructure

Table 2 reports the mean values of the microstructural parameters resulting from the image analysis, while Figure 2a–d shows selected micrographs of the HSiSDIs analyzed.

**Table 2**
Microstructure analysis results of the investigated HSiSDI of 4.2 wt.% Si content produced through different molds

| Mold | Nodularity [%] | Nodule Count [Nr/mm$^2$] | Nodule size [μm] | Chunky graphite |
|---|---|---|---|---|
| L25 mm | 74.4 ±1.8 | 149.8 ±1.9 | 18.6 ±0.4 | No |
| Y25 mm | 85.4 ±1.1 | 210.6 ±2.0 | 20.0 ±0.3 | No |
| Y50 mm | 82.2 ±1.3 | 125.6 ±2.0 | 26.2 ±0.5 | Traces |
| Y75 mm | 83.3 ±1.0 | 107.3 ±1.9 | 28.5 ±0.6 | Traces |

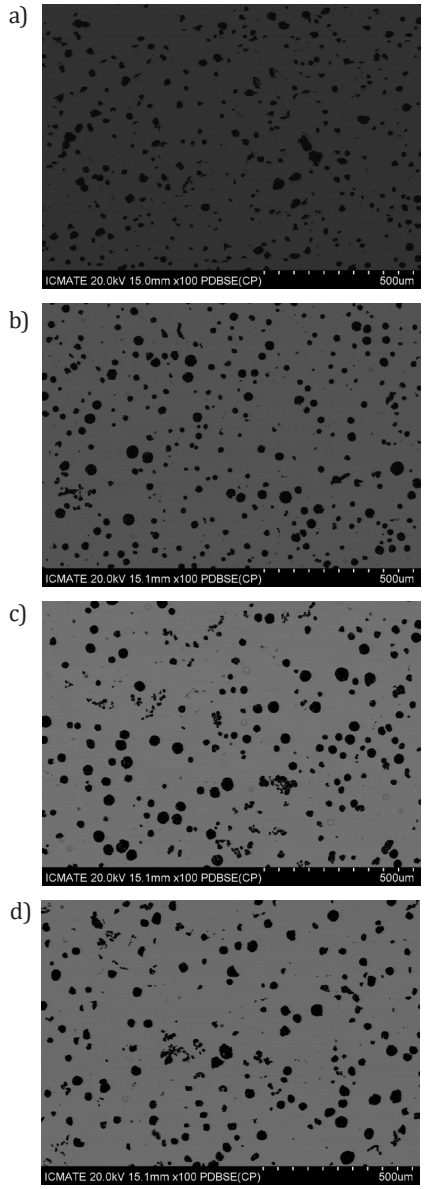


**Fig. 2.** Back Scattered Electron Imaging micrographs of HSiSDIs, with 4.2 wt.% of Si content, produced through: a) 25 mm Lynchburg; b) 25 mm Y-block; c) 50 mm Y-block; d) 75 mm Y-block molds

According to these data, the microstructure of the ductile irons produced through a Lynchburg mold of 25 mm (L25 mm) diameter shows the lowest nodularity and degenerated graphite aggregates. Samples Y25 mm shows greater nodularity, although graphite degeneration is also observable in this case. Increasing the thickness (samples Y50–Y75 mm) a reduction of the nodularity is observed. Furthermore, the appearance of chunky graphite is seen in Figure 2c, d.

### 3.2. Strain hardening analysis results, and MAD and IAD analysis

According to the Voce approach it was possible to define the strain hardening parameters $1/\varepsilon_c$ and $\Theta_o$ necessary to define the Matrix Assessment Diagram (MAD) reported in Figure 3 for Y50–Y75 mm samples. For comparison purposes, the graph also reports the data provided by a previous research [15] aimed to study the strain hardening behavior of HSiSDIs samples with various Si content, i.e. 3.5 wt.% and 4.5 wt.%, produced through Y50–Y75 mm molds [15].

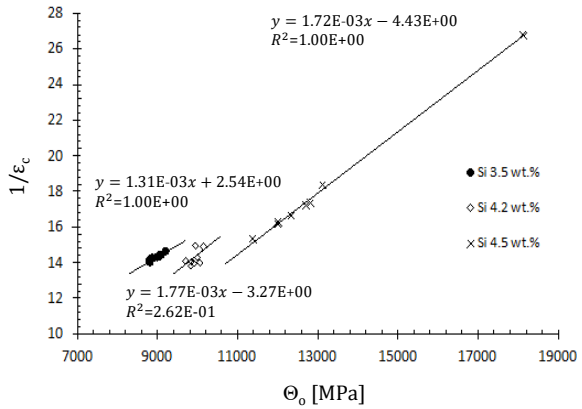


**Fig. 3.** Matrix Assessment Diagram (MAD) of Y50–Y75 mm HSiSDIs with Si content of 4.2 wt.%. For comparison, the data of a previous research [15] on HSiSDI samples with 3.5 wt.% and 4.5 wt.% are reported

The Voce parameters related to the three different kind of specimens, i.e 3.5, 4.2 and 4.5 wt.% Si content respectively, characterized by different chemical composition, lied in a specific region of MAD and on a specific line, namely $1/\varepsilon_c = m\Theta_o + C$. According to the Voce approach, $\sigma_V$ defines the strenght of the material and it is related to Voce parameters through the expression:

$$\sigma_V = \varepsilon_c \cdot \Theta_o \tag{3}$$

so, $\sigma_V$ can be rewritten as $\sigma_V = \Theta_o/(m\Theta_o + C)$. Consistently with the physical meaning of the Voce equation [38–41], the intercept of the best fittng line gives information on the integrity of the tested material. Considering the data of samples with a Si content of 3.5 wt.% [15], the intercept is positive. Thus, $\sigma_V$ grows with increasing $\Theta_o$. The latter is correlated to the microstructure of the material: complying with plasticity theory, greater values of $\Theta_o$ (thus $\sigma_V$) are associated to finer microstructure and so to a stronger materials as demonstrated in a previous study [42, 43] on GJS400 with a conventional Si content of 2.5 wt.%.

However, according to Figure 3, samples with a Si content of 4.2 wt.% up to 4.5 wt.% show corresponding best fitting line with a negative intercept value that decreases with increasing the Si content. Remembering the aforesaid definition of saturation stress $\sigma_v$, the negative value of the intercept C results in a reduction of $\sigma_V$ increasing $\Theta_o$. This result is in contrast with Voce physical meaning and plasticity theories. It has been reported [44] that the presence of defects affects the plastic behavior of the material describing an unexpected regular trend, i.e. *defect-driven plasticity*, rather than a random influence as expected.

In Figure 4, data of HSiSDI samples with 4.2 wt.% Si content are reported comparing Lynchburg and Y-block molds. According to MAD, specimens produced through small thickness (25 mm Lynchburg and Y-block molds) show a positive intercept of the best fitting line. On the other hand, samples produced with 50–75 mm Y-molds show a negative intercept, so suggesting that the HSiSDIs produced with faster cooling rates is sound, while with slower cooling rates the material is affected by defects according to the defects-driven-plasticty hypothesis.

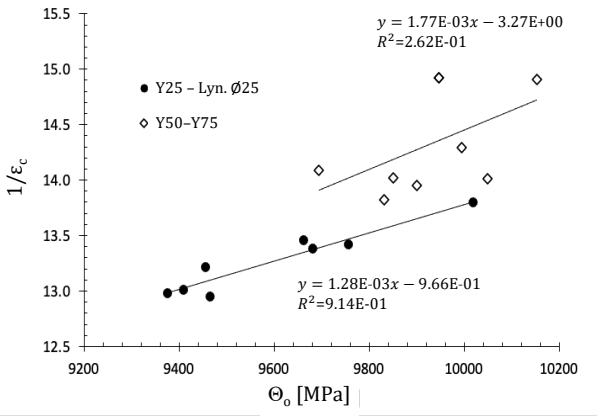


**Fig. 4.** Matrix Assessment Diagram (MAD) of HSiSDIs with Si content of 4.2 wt.% produced through Lynchburg and Y-block molds

Figure 5 reports the Integrity Assessment Diagram (IAD), defined as $\varepsilon_{rupture}$ vs. $\varepsilon_{uniform}$. The dashed line represents the dicotomy line, where $\varepsilon_{rupture} = \varepsilon_{uniform}$, and defines the occurrence of necking. The data points where $\varepsilon_{rupture} < \varepsilon_{uniform}$ are related to early failures due to the presence of metallurgical defects or metallurgical discontinuity, while the points where $\varepsilon_{rupture} > \varepsilon_{uniform}$ are related to sound materials. Specimens with 4.2 wt.% Si produced through 25 mm Lyncburg and Y-molds lie above the dicotomy line, so beyond necking, and show a mean value of elongation to rupture of 0.16 ±0.01, where the error is the standard deviation. Decrasing the cooling rates (50–75 mm Y-blocks), in IAD it is observed a certain variability of the data, which seems to be related to the soundness of the material. Furthermore, compared to 25 mm samples, these data show a reduction of the elongation to rupture to an average value of 0.11 ±0.04 that, evidently, is not due to the high Si content which remain unchanged between the specimens. Thus the key role of the possible presence of metallurgical defects on the definition of the tensile plastic behavior of the material under analysis can be confirmed.

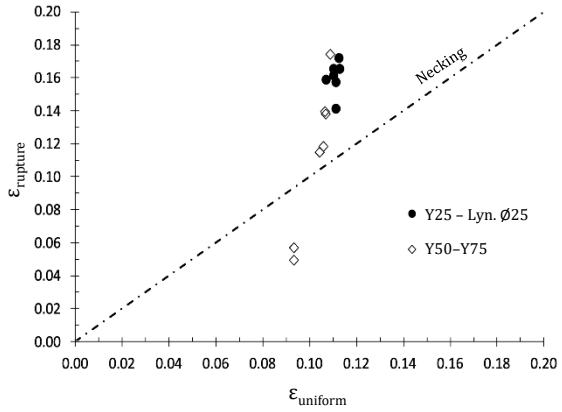


**Fig. 5.** Integrity Assessment Diagram (IAD) of HSiDIs with 4.2 wt.% Si produced through Lynchburg and Y-block molds

## 4. DISCUSSION

In the present investigation, HSiSDI samples with a Si content of 4.2 wt.% produced through different molds, so with different cooling rates, were analyzed. According to Figure 2 and the data reported in Table 2, the graphite parameters were consistent to the values found for Si 3.5 wt.% and 4.5 wt.% reported elsewhere [15]. Nodularity was good for all cooling rates, with a slightly lower value for the Lynchburg mold, suggesting that no significant graphite degeneracy was present for all solidification times. In fact chunky graphite was found in traces only for the slower cooling rates (50–75 mm Y-blocks), consistently with literature [4, 25–27] where it has been reported that Si and slow solidification rates promote the formation of chunky graphite.

According to Figure 3, where data of the present research were compared with the results of a previous study [15] on other two HSiSDIs with different Si contents, MAD can identify the different grades of ductile iron since three different lines corresponding to three different contents of Si are found. MAD can give information also about the microstructure soundness of the materials, which is correlated to the plastic behavior according to the defect-drive-plasticity theory. Specimens with a Si content of 3.5 wt.% [15] show a fitting line having a positive intercept (C = +2.54), indicating soundness of the material [39–45]. Conversely, for a Si content of 4.5 wt.% [15], the intercept of the best fitting line is negative (C = −4.43), suggesting the presence of chunky graphite as reported in [15]. So, according the the defect-driven-plasticity hypotesis, the negative intercept (C = −3.27) of the Si 4.2 wt.% suggests the presence of some defects.

In Figure 4, a close up of 4.2 wt.% Si MAD data is reported. For longer solidification times, i.e. Y50-75 mm, not only the intercept of the linear fit is negative (C = −3.27), but the data show also a significant scattering and low $R^2$, equal to 0.26. Furthermore, the data corresponding to the faster cooling rates (25 mm Lynchburg and Y-block) show a positive intercept (C = +0.97) of the best fitting line, suggesting the soundness of the material. It is noteworthy that the behaviour observed is absolutely consistent with the MAD trend of Si 4.5 wt.% samples reported in [15], which was related to

significant fraction of chunky graphite found in the HSiSDIs produced with slow cooling rates.

The IAD in Figure 5 shows that the microstructure of samples produced through 25 mm Lynchburg and 25 mm Y-block molds, have higher strains to failure with respect the values of 50–75 mm Y-blocks specimens. Furthermore, since $\varepsilon_{rupture} > \varepsilon_{uniform}$, it is newly suggested the integrity of the material, whilst for 50–75 mm Y-blocks specimens not all data are above the dichotomy line of necking. This finding indicates that some defects are present in the HSiSDIs produced with longer solidification time, which is consistent with the negative value of the intercept C in MAD. By comparing these findings with the results of Si 4.5 wt.% HSiSDIs reported in [15], where significant content of chunky graphite was found, the analogy is very strong, suggesting that the defects that most define the Si 4.2 wt.% behaviour in MAD are the traces of chunky graphite. Indeed, several data points are above the dichotomy line, suggesting the absence of defects and a good plastic behaviour. So the traces of chunky graphite give rise to a wide variability of MAD behaviour. So the unpredictability of the HSiSDIs with 4.2 wt.% Si produced with slower cooling rates may be a negative consequence.

So the presence in traces of chunky graphite have some negative effects on the quality of Si 4.2 wt.% HSiSDIs produced with longer solidification times (Y-molds of 50–75 mm thickness). The quality assessment procedure based on Voce analysis (MAD and IAD) seems to be very sensitive and capable of identifying its adverse effects even if the microstructure parameters reported in Table 2 comply with standard EN 1563:2018. Indeed, chemical ordering is also believed to be deleterious in HSiSDIs with increasing Si [7, 8]. However, since there is no reason to believe that cooling rates can affect chemical ordering, chunky graphite appears to be the reliable explanation of the defect-driven-plasticity effects pointed out in MAD and IAD for HSiSDIs with Si content of 4.2 wt.%.

## 5. CONCLUSIONS

In the present work different samples of HSiSDI with a Si content of 4.2 wt.%, produced through different molds, thus different solidification rates, were studied in order to evaluate the correlation between the microstructure and the tensile mechanical properties through Voce analysis. Four different cooling rates were explored to produce the HSiSDIs. The microstructural characterization was performed using a high resolution SEM and the image analysis was conducted complying standard ASTM E2567-16a. The tensile mechanical behavior was investigated according to Voce approach, so modelling the tensile flow curves through Voce constitutive equation. Voce parameters $1/\varepsilon_c$ and $\Theta_o$ were determined and used to define the MAD. Furthermore, it was possible to define the IAD that allows to identify the eventual premature failures of the tensile tested materials. According to the experimental results obtained, the following consideration can be made:

- MAD allows the univocal identification of the tested material since, through the comparison with result of a previous study [15], three different best fitting lines corresponding to three different contents of Si are found;
- the intercept of the data best fitting line in MAD of the 25 mm Lynchburg and 25 mm Y-block samples with a Si content of 4.2 wt.% is positive, according to Voce equation physical meaning and plasticity theories. So, the tensile plastic behavior observed comply with the fact that increasing $\sigma_V$ and $\sigma_0$ determine an increment of $\Theta_o$, which is correlated to the microstructure of the material;
- the negativity of the intercept of the data best fitting line in MAD of 50–75 mm Y-blocks specimens is not coherent with physical meaning of Voce equation and plasticity theories, with the result of a singular tensile mechanical behavior for which decreasing $\sigma_V$ determines an increase of $\Theta_o$ with $\sigma_0$ constant;
- the MAD data of Y50–Y75 mm samples, i.e. those produced through the slowest cooling rates, show a significant scattering with low $R^2$. Furthermore, these specimens show a reduction of the elongation to failure and, in some cases, premature ruptures occurred before necking;
- according to IAD, data of specimens produced through 25 mm Lynchburg and Y-block molds, lie beyond necking; thus premature ruptures did not occur;
- the plastic behavior shown by 25 mm Lynchburg and 25 mm Y-block samples is correlated to the optimal structural integrity of the microstructure;
- the unusual behavior of 50–75 mm Y-block samples was affected by the presence of metallurgical defects, in particular by the presence of degenerated graphite;
- considering the results obtained, it can be stated that the quality assessment procedure based on the Voce approach is clearly sensitive and capable of identifying the presence of defects and metallurgical discontinuities; furthermore, this procedure has proved capable of highlighting the negative effects of such defects on the quality of the material and thus demonstrating its usefulness.

## REFERENCES

[1] Weiβ P., Brachmann J., Bührig-Polaczek A. & Fischer S.F. (2015). Influence of nickel and cobalt on microstructure of silicon solution strengthened ductile iron. *Materials Science and Technology*, 31(12), 1479–1485. Doi: https://doi.org/10.1179/1743284714Y.0000000735.

[2] de la Torre U., Loizaga A., Lacaze J. & Sertucha J. (2014). As cast high silicon ductile irons with optimised mechanical properties and remarkable fatigue properties. *Materials Science and Technology*, 30(12), 1425–1431. Doi: https://doi.org/10.1179/1743284713Y.0000000483.

[3] Sertucha J., Lacaze J., Serrallach J., Suárez R. & Osuna F. (2012). Effect of alloying on mechanical properties of as cast ferritic nodular cast irons. *Materials Science and Technology*, 28(2), 184–191. Doi: https://doi.org/10.1179/1743284711Y.0000000014.

[4] Stets W., Löblich H., Gassner G. & Schumacher P. (2014). Solution strengthened ferritic ductile cast iron properties, production and application. *International Journal of Metalcasting*, 8(2), 35–40. Doi: https://doi.org/10.1007/BF03355580.

[5] Björkegren L.E., Hamberg K. & Johannesson B. (1996). Mechanical properties and machinability of Si-solution-hardened ferritic ductile iron. *AFS Transactions*, 104, 139–145.

[6] Khalil-Allafi J. & Amin-Ahmadi B. (2011). Influence of mold preheating and silicon content on microstructure and casting properties of ductile iron in permanent mold. *Journal of Iron and Steel Research International*, 18(3), 34–39. Doi: https://doi.org/10.1016/S1006-706X(11)60034-4.

[7] González-Martíneza R., de la Torre U., Lacaze J. & Sertucha J. (2018). Effects of high silicon contents on graphite morphology and room temperature mechanical properties of as-cast ferritic ductile cast irons. Part I – Microstructure. *Materials Science Engineering: A*, 712, 794–802. Doi: https://doi.org/10.1016/j.msea.2017.11.050.

[8] González-Martínez R., de la Torre U., Ebelb A., Lacaze J. & Sertucha J. (2018). Effects of high silicon contents on graphite morphology and room temperature mechanical properties of as-cast ferritic ductile cast irons. Part II – Mechanical properties. *Materials Science Engineering: A*, 712, 803–811. Doi: https://doi.org/10.1016/j.msea.2017.11.051.

[9] Bradley W.L. & Srinivasan M.N. (1990). Fracture and fracture toughness of cast irons. *International Materials Reviews*, 35(1), 129–161. Doi: https://doi.org/10.1179/095066090790324028.

[10] Angus H.T. (1976). Cast Iron: Physical and Engineering Properties (Second Edition). Butterworth-Heinemann.

[11] Lacaze J., Larrañaga P., Asenjo I., Suárez R. & Sertucha J. (2012). Influence of 1 wt% addition of Ni on structural and mechanical properties of ferritic ductile irons. *Materials Science and Technology*, 28(5), 603–608. Doi: https://doi.org/10.1179/1743284711Y.0000000100.

[12] Alhussein A., Risbet M., Bastien A., Chobaut J.P., Balloy D. & Favergeon J. (2014). Influence of silicon and addition elements on the mechanical behavior of ferritic cast iron. *Materials Science Engineering: A*, 605, 222–228. Doi: https://doi.org/10.1016/j.msea.2014.03.057.

[13] Glavas Z., Strkalj A. & Stojakovich A. (2016). The properties of silicon alloyed ferritic ductile irons. *Metalurgija*, 55(3), 293–296.

[14] Fairhurst W. & Röhrig K. (1979). High-silicon nodular irons. *Foundry Trade Journal*, 146, 657–681.

[15] Angella G., Donnini R. & Zanardi F. (2020). Assessment of microstructure effects on tensile behaviour in silicon strengthened ductile irons produced through different cooling rates. *International Journal of Cast Metals Research*, 33(2–3), 89–102. Doi: https://doi.org/10.1080/13640461.2020.1757917.

[16] Karsay S.I. & Campomanes E. (1970). Control of graphite structure in heavy ductile iron castings. *AFS Transactions*, 78, 85–92.

[17] Lacaze J., Magnusson-Åberg L. & Sertucha J. (2013). Review of microstructural features of chunky graphite in ductile cast irons. Keith Millis World Symposium on Ductile Cast Iron: 15–17 October, Nashville. Red Hook (NY): Curran, 360–368.

[18] de la Torre U., Lacaze J. & Sertucha J. (2016). Chunky graphite formation in ductile cast irons: effect of silicon, carbon and rare earths. *International Journal of Materials Research*, 107(11), 1041–1050. Doi: https://doi.org/10.3139/146.111434.

[19] Bauer B., Pokopec I. M., Petrič M. & Mrvar P. (2017). Effect of Si and Ni addition on spheroidal morphology in heavy section spheroidal graphite iron parts. *Materials Science Forum*, 925, 70–77. Doi: https://doi.org/10.4028/www.scientific.net/MSF.925.70.

[20] Gagné M. & Argo D. (1987). Heavy section ductile iron castings – Part I: Structure and properties. Advanced Casting Technology: 12–14 November, Kalamazoo. ASM International, 231–244.

[21] Källbom R., Hamberg K. & Björkegren L.E. (2005). Chunky-graphite – formation and influence on mechanical properties in ductile cast iron. In: J. Samuelson, G. Marquis, J. Solin (Eds.). Competent Design by Castings: Improvements in a Nordic Project, 13–14 June. Espoo. Helsinki.

[22] Celis M.M., Domengès B., Hug E. & Lacze J. (2018). Analysis of nuclei in a heavy-section nodular iron casting. *Materials Science Forum*, 925, 173–180. Doi: https://doi.org/10.4028/www.scientific.net/MSF.925.173.

[23] Minnebo P., Nilsson K.F. & Blagoeva D. (2007). Tensile, compression and fracture properties of thick-walled ductile cast iron components. *Journal of Material Engineering and Performance*, 16(1), 35–45. Doi: https://doi.org/10.1007/s11665-006-9005-z.

[24] Borsato T., Ferro P., Berto F. & Carollo C. (2016). Mechanical and fatigue properties of heavy section solution strengthened ferritic ductile iron castings. *Advanced Engineering Materials*, 18(12), 2070–2075. Doi: https://doi.org/10.1002/adem.201600256.

[25] Goodrich G.M. & Lobenhofer R.W. (2002). Effect of cooling rate on ductile iron mechanical properties. *AFS Transactions*, 110, 1003–1032.

[26] Hsu G.H., Chen M.L. & Hu C.J. (2007). Microstructure and mechanical properties of 4% cobalt and nickel alloyed ductile irons. *Materials Science Engineering: A*, 444 (1–2), 339–346. Doi: https://doi.org/10.1016/j.msea.2006.09.027.

[27] Serrallach J., Lacaze J., Sertucha J., Suárez R. & Monzón A. (2011). Effect of selected alloying elements on mechanical properties of pearlitic nodular cast irons. Key Engineering Materials, 457, 361–366. Doi: https://doi.org/10.4028/www.scientific.net/KEM.457.361.

[28] Tartaglia J.M., Gundlach R.B. & Goodrich G.M. (2014). Optimizing structure-property relationships in ductile iron. *International Journal of Metalcasting*, 8 (4), 7–38. Doi: https://doi.org/10.1007/BF03355592.

[29] Ceschini L., Morri Al., Morri An., Salsi E., Squatrito R., Todaro I. & Tomesani L. (2015). Microstructure and mechanical properties of heavy section ductile iron castings: experimental and numerical evaluation of effects of cooling rates. *International Journal of Cast Metals Research*, 28(6), 365–374. Doi: https://doi.org/10.1179/1743133615Y.0000000022.

[30] Zanardi F., Bonollo F., Bonora N., Ruggiero A. & Angella G. (2017). A contribution to new material standards for Ductile Irons and Austempered Ductile Irons. *International Journal of Metalcasting*, 11(1), 136–147. Doi: https://doi.org/10.1007/s40962-016-0095-6.

[31] Ductile Iron Data for Design Engineers – Section III. Engineering Data (Part 1) Tensile Properties: Relationships between Tensile Properties. Retreived from: https://ductile.org [accesed 13 July 2019].

[32] Rivera G., Boeri R. & Sikora J. (2003). Influence of the inoculation process, the chemical composition and the cooling rate, on the solidification macro and microstructure of ductile iron. *International Journal of Cast Metals Research*, 16 (1–3), 23–28. Doi: https://doi.org/10.1080/13640461.2003.11819553.

[33] Stefanescu D.M., Ruxanda R. & Dix L.P. (2003). The metallurgy and tensile mechanical properties of thin wall spheroidal graphite irons. *International Journal of Cast Metals Research*, 16(1–3), 319–324. Doi: https://doi.org/10.1080/13640461.2003.11819602.

[34] Pan Y.-N., Lin C.-C. & Chang R.-M. (2012). Assessments of relationship between microstructures and mechanical properties for heavy section ductile cast irons. *International Journal of Cast Metals Research*, 25(5), 301–306. Doi: https://doi.org/10.1179/1743133612Y.0000000027.

[35] Donnini R., Zanardi F., Vettore F. & Angella G. (2018). Evaluation of microstructure quality in ductile irons based on tensile behaviour analysis. *Materials Science Forum*, 925, 342–349. Doi: https://doi.org/10.4028/www.scientific.net/MSF.925.342.

[36] Angella G. & Zanardi F. (2018). Microstructure quality assessment of isothermed ductile irons through tensile tests. 73rd World Foundry Congress "Creative Foundry": 23–27 September. Krakow. Krakow: Stowarzyszenie Techniczne Odlewników Polskich, 265–266.

[37] Angella G. & Zanardi F. (2019). Validation of a New Quality Assessment Procedure for Ductile Irons Production Based on Strain Hardening Analysis. *Metals*, 9(8), 837–850. Doi: https://doi.org/10.3390/met9080837.

[38] Estrin Y. (1996). Dislocation density related constitutive modelling. In: A. Krausz, K. Krausz, Unified Constitutive Laws of Plastic Deformation, 1. New York: Academic Press, 69–106.

[39] Kocks U.F. & Mecking H. (2003). Physics and phenomenology of strain hardening: the FCC case. *Progress in Materials Science*, 48(3), 171–273. Doi: https://doi.org/10.1016/S0079-6425(02)00003-8.

[40] Angella G., Zanardi F. & Donnini R. (2016). On the significance to use dislocation-density-related constitutive equations to correlate strain hardening with microstructure of metallic alloys: The case of conventional and austempered ductile irons. *Journal of Alloys and Compounds*, 669, 262–271. Doi: https://doi.org/10.1016/j.jallcom.2016.01.233.

[41] Angella G. & Zanardi F. (2018). Comparison among Different Constitutive Equations on Investigating Tensile Plastic Behavior and Microstructure in Austempered Ductile Iron. *Journal of Casting & Materials Engineering*, 2(1), 14–23. Doi: https://doi.org/10.7494/jcme.2018.2.1.14.

[42] Angella G., Masaggia S., Ripamonti D., Górny M. & Zanardi F. (2019). The role of microstructure on tensile plastic behaviour of ductile iron GJS 400 produced through different cooling rates, Part I: Microstructure. *Metals*, 9(12), 1282. Doi: https://doi.org/10.3390/met9121282.

[43] Angella G., Donnini R., Ripamonti D., Górny M. & Zanardi F. (2019). The role of microstructure on tensile plastic behaviour of ductile iron GJS 400 produced through different cooling rates, Part II: Tensile Modelling. *Metals*, 9(9), 1019. Doi: https://doi.org/10.3390/met9091019.

[44] Angella G., Cova M., Berutzzi G. & Zanardi F. (2020). Soundness Discrimination in Ferrite Ductile Irons through Tensile Data Analysis. *International Journal of Metalcasting*, 14(3), 816-826. Doi: https://doi.org/10.1007/s40962-020-00435-0.

[45] Estrin Y. (1998). Dislocation theory based constitutive equation modelling: foundation and application. *Journal of Materials Processing and Technology*, 80–81, 33–39. Doi: https://doi.org/10.1016/S0924-0136(98)00208-8.